Numerical Investigation of Effects of Silt Particles with Different Mean Diameters on Cavitation Flow Evolution in the Nozzle

Xiangdong Han(✉) and Fangyan Yu

School of Civil Engineering, Nanchang Institute of Technology, Nanchang 330044, China
fluidhanxd@126.com

Abstract. Effects of silt particles with various mean diameters on cavitation development in the nozzle were numerically investigated. The diameters were 0.0015 mm, 0.0035 mm, and 0.0055 mm, respectively. Results clearly indicated that vapor contents in silt particle-water cavitation flow were greater than that of pure water cavitation flow. Cavitation development in the nozzle was promoted by silt particles with different mean diameters. Maximum and absolute minimum slip velocities were higher than in pure water cavitation flow. Also, maximal and minimal turbulent kinetic energies were greater than that of pure water cavitation flow. Slip velocity and turbulent kinetic energy were primary factors to influence silt particle-water cavitation flow evolution in the nozzle.

Keywords: Cavitation flow · mean diameter · vapor content · slip velocity · turbulent kinetic energy

1 Introduction

Cavitation is one kind of multi-phase and complex physical phenomena [1]. It always appears in many different fluid-handling facilities [2], which includes pump [3], hydro-turbine [4], nozzle [5], and propeller [6]. The evolution is affected by the variations of velocity and pressure [7], which are in turn influenced by the alternations of surface roughness [8], boundary condition [9], and viscosity [10].

For the natural rivers and oceans, they have silt particles more or less. Under this kind of operation environment, cavitation in the fluid-handling facilities is deeply affected by silt particles, one kind of silt particle-water cavitation flow (SPWCF). The most remarkable characteristic is the complex coupling among silt particles, water, with vapor [11–13].

Some scholars investigated silt particle abrasion and cavitation erosion caused by SPWCF and the interactions between one solid particle with one cavitation bubble under small scale condition. Representative literatures were that:

Hu et al. [14] discussed effects of particle concentrations on the synergistic destruction for stainless steel 304, which was assessed by variations of mass loss, scanning electron microscopy, roughness, and surface residual stress. Li [15] put forward one

L. Yan and J. Na (Eds.): ICFPMCE 2022, AHE 10, pp. 14–24, 2023.
https://doi.org/10.2991/978-94-6463-022-0_3

new model which was named of an envisaged micro model to predict the co-damage of silt particle abrasion and cavitation erosion; via the analysis, one meritorious conclusion he obtained was that cavitation erosion was stimulated by silt particle abrasion. Zuo et al. [16] got the single particle motion characteristics, driven by one bubble which was induced by laser. Xu et al. [17] investigated one particle motion characteristics driven by one single cavitation bubble; they got that particle velocity had close relation with liquid viscosity and particle size.

However, investigations on the effects of silt particles with diverse mean diameters under large scale conditions on cavitation evolution were particularly few. Related laws and mechanisms were not determined as well. Therefore, we performed the corresponding numerical simulations.

2 Numerical Methods

2.1 Fundamental Equations

To perform the numerical simulation of SPWCF in the nozzle by ANSYS-Fluent, primary phase was the water; secondary phase includes vapor and silt particles. Phase change occurs between water with vapor; for silt particles, this process is ignored. Water and vapor own the same velocity and pressure fields. Silt particles are taken as pseudo-fluid due to the minute mean diameters. Continuity equation, momentum equation, transportation equation, and relative velocity equation [18] are shown by the follows.

$$\frac{\partial \rho_{\mathrm{m}}}{\partial t} + \frac{\partial \left(\rho_{\mathrm{m}} u_j\right)}{\partial x_j} = 0 \tag{1}$$

$$\frac{\partial (\rho_{\mathrm{m}} u_i)}{\partial t} + \frac{\partial \left(\rho_{\mathrm{m}} u_i u_j\right)}{\partial x_j} = -\frac{\partial p}{\partial x_i} + \frac{\partial}{\partial x_j}\left(\mu_{\mathrm{m}} \frac{\partial u_i}{\partial x_j}\right) \tag{2}$$

$$\frac{\partial \rho_{\mathrm{l}} \alpha_{\mathrm{l}}}{\partial t} + \frac{\partial \left(\rho_{\mathrm{l}} \alpha_{\mathrm{l}} u_j\right)}{\partial x_j} = R = R_{\mathrm{e}} - R_{\mathrm{c}} \tag{3}$$

$$\frac{\partial \rho_{\mathrm{v}} \alpha_{\mathrm{v}}}{\partial t} + \frac{\partial \left(\rho_{\mathrm{v}} \alpha_{\mathrm{v}} u_j\right)}{\partial x_j} = -R \tag{4}$$

$$\frac{\partial \rho_{\mathrm{s}} \alpha_{\mathrm{s}}}{\partial t} + \frac{\partial \left(\rho_{\mathrm{s}} \alpha_{\mathrm{s}} u_j\right)}{\partial x_j} = 0 \tag{5}$$

$$\mathbf{v}_{pq} = \mathbf{v}_p - \mathbf{v}_q \tag{6}$$

where ρ_{m} is the mixture density and u is the mixture velocity. x is coordinate; subscripts i and j are 1, 2, and 3. t is time. p is local pressure. ρ_{l}, ρ_{v}, and ρ_{s} are the densities of water, vapor, and silt particles, respectively; α_{l}, α_{v}, and α_{s} are the corresponding concentrations. μ_{m} is the mixture dynamic viscosity. R is the net source term, R_{e} is the evaporization source term, and R_{c} is the condensation source term. V_{pq} is the relative velocity between primary phase and secondary phase; V_{p} is the velocity of primary phase, which is the water velocity in SPWCF; V_{q} is the velocity of secondary phase; it is the velocity of vapor and silt particles, respectively.

2.2 Turbulent Model

SST k-ω turbulent model [19] is used to solve the turbulent flow in the nozzle. Merits of primal k-ε and k-ω turbulent models are integrated to form this model. Equations for turbulent kinetic energy and specific dissipation rate are shown as follows.

$$\rho\frac{\partial k}{\partial t}+\rho\overline{u_j}\frac{\partial k}{\partial x_j}=P_k-\rho\beta_*\omega k+\frac{\partial}{\partial x_j}\left[\left(\mu+\frac{\mu_t}{\sigma_k}\right)\frac{\partial k}{\partial x_j}\right] \tag{7}$$

$$\begin{aligned}\rho\frac{\partial \omega}{\partial t}+\rho\overline{u_j}\frac{\partial \omega}{\partial x_j}&=\alpha P_\omega-\rho\beta\omega^2+\frac{\partial}{\partial x_j}\left[\left(\mu+\frac{\mu_t}{\sigma_\omega}\right)\frac{\partial \omega}{\partial x_j}\right]\\&+2\rho(1-F_B)\frac{1}{\sigma_{\omega_{\text{out}}}\omega}\frac{\partial k}{\partial x_j}\frac{\partial \omega}{\partial x_j}\end{aligned} \tag{8}$$

where k is turbulent kinetic energy and ω is the specific dissipation rate; P_k and P_ω are the corresponding production terms. F_B is one blending function. μ is dynamic viscosity and μ_t is the turbulent viscosity. β_* and $\sigma_{\omega\text{out}}$ are model constants, taken as 0.09 and 1.168.

2.3 Cavitation Model

Schnerr-Sauer cavitation model [20] is employed to perform the phase change between water with vapor of PWCF and SPWCF. The primary merit is that empirical coefficients do not appear in this model; therefore, the prediction accuracy is relatively high. The source terms are as follows:

$$R_\text{e}=\frac{\rho_\text{v}\rho_\text{l}}{\rho_{\text{m - 1}}}\alpha_\text{v}(1-\alpha_\text{v})\frac{3}{r_\text{b}}\sqrt{\frac{2}{3}\frac{p_\text{v}-p}{\rho_\text{l}}} \tag{9}$$

$$R_\text{c}=\frac{\rho_\text{v}\rho_\text{l}}{\rho_{\text{m - 1}}}\alpha_\text{v}(1-\alpha_\text{v})\frac{3}{r_\text{b}}\sqrt{\frac{2}{3}\frac{p-p_\text{v}}{\rho_\text{l}}} \tag{10}$$

where $\rho_{\text{m-1}}$ is the mixture density of water and vapor, r_b is the radius of one cavitation bubble, and P_v is the saturated vapor pressure.

3 Numerical Simulation Setup

3.1 Physical Model

One nozzle was employed to perform the numerical simulations of PWCF and SPWCF with different silt particle mean diameters, provided by Nurick [21]. Main geometrical sizes were that inlet diameter was 23 mm, outlet diameter was 8 mm, total length was 48 mm, and length of the orifice was 32 mm, respectively (Fig. 1).

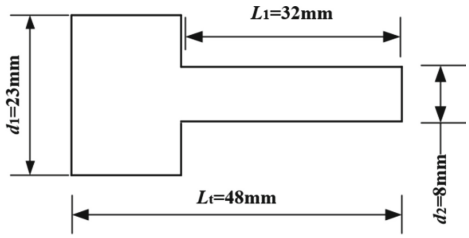

Fig. 1. Physical model.

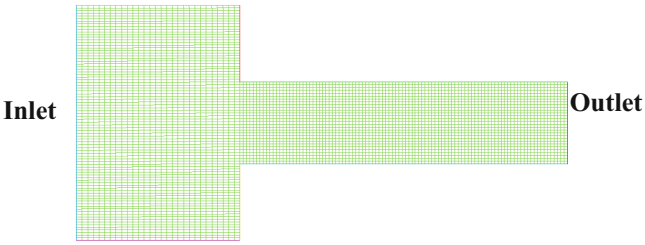

Fig. 2. Mesh generation.

3.2 Mesh Generation

Quadrilateral structured meshes were employed to discretize the nozzle computational domain. Cavitation bubbles mainly concentrated in the orifice; therefore, the corresponding meshes were refined. The total number was 55346 (Fig. 2).

3.3 Material Properties and Boundary Conditions

For water, the density was $\rho_l = 1000$ kg/m^3 and the viscosity was $\mu_l = 0.001$ kg/m-s. Vapor density was $\rho_v = 0.02558$ kg/m^3 and corresponding viscosity was $\mu_v = 1.26 \times 10^{-6}$ kg/m-s. Silt particle density was $\rho_s = 2650$ kg/m^3. Silt particle mean diameter was $d_s = 0.0015$ mm, 0.0035 mm, and 0.0055 mm and the concentration was $\alpha_s = 1\%$.

At inlet, it was pressure-inlet boundary condition. The value was 250,000,000 Pa. For outlet, it was set as pressure-outlet boundary condition. The value was 95,000 Pa. All nozzle walls were non-slip.

SPWCF in the nozzle was unsteady flow. According to CFL condition, the time step was determined as $\Delta t = 1.5 \times 10^{-6}$ s.

4 Results and Discussion

4.1 Distributions of Vapor Volume Fraction

Case of SPWCF with $d_s = 0.0015$ mm and $\alpha_s = 1\%$ was employed to analyze the vapor volume fraction distribution in the nozzle, shown in Fig. 3.

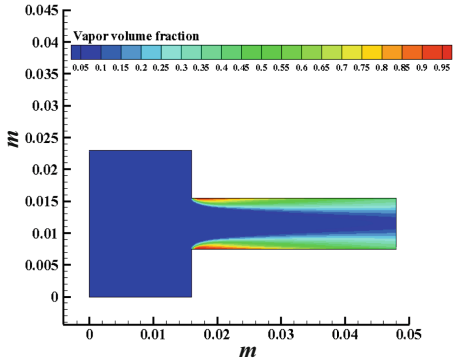

Fig. 3. Distributions of vapor volume fraction in the nozzle ($d_s = 0.0015$ mm and $\alpha_s = 1\%$).

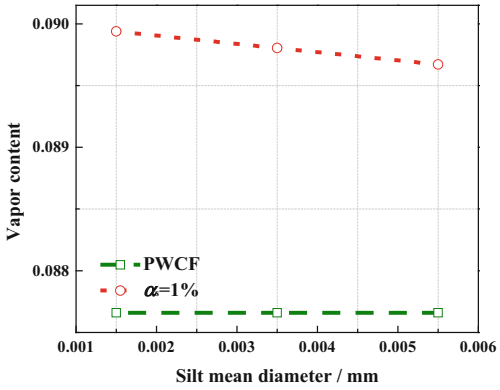

Fig. 4. Variations of vapor content in SPWCF and PWCF.

The distribution was axisymmetric. At the beginning part of the nozzle, vapor volume fraction was especially low. At the orifice, the vapor volume fraction was very high, particularly at the beginning segment.

4.2 Variations of Vapor Content

Vapor content is one significant index to measure cavitation development degree. Under all silt mean diameter with $\alpha_s = 1\%$ conditions, all vapor contents of SPWCF were greater than that of PWCF. Silt particles promoted cavitation evolution in the nozzle (Fig. 4).

5 Reasons and Explanation

5.1 Variations of Slip Velocity

Distributions of slip velocity under PWCF and SPWCF with $d_s = 0.0015$ mm and $\alpha_s = 1\%$ is shown in Fig. 5.

High-level slip velocities were at regions where vapor volume fractions were particularly high; it meant that slip velocity had critical effects on cavitation development in the nozzle.

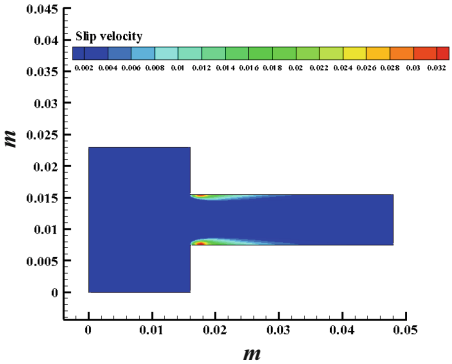

(a) PWCF

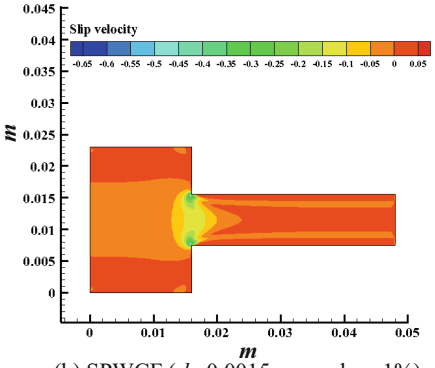

(b) SPWCF (d_s=0.0015mm and α_s=1%)

Fig. 5. Distributions of slip velocity.

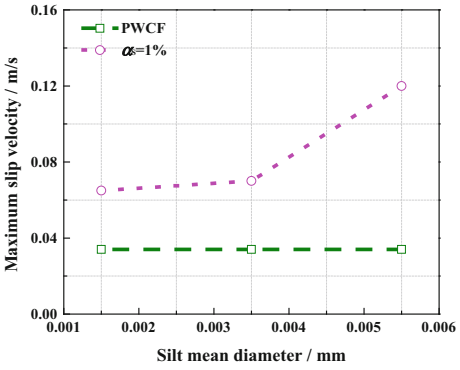

(a) Maximum

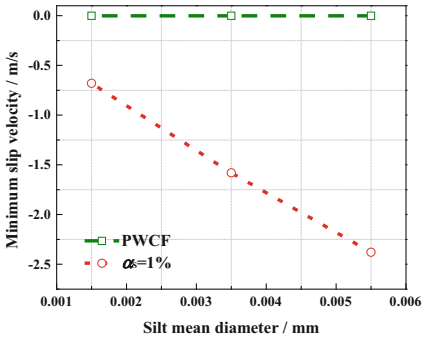

(b) Minimum

Fig. 6. Variations of maximum and minimum slip velocities under different silt mean diameter conditions.

Maximal and minimal slip velocities of SPWCF under all silt mean diameters were compared with the corresponding ones of PWCF. For SPWCF, all maximum slip velocities were greater than in PWCF. While for minimal ones, they were that the absolute values were higher than in PWCF. Variations of maximal and minimal slip velocities in SPWCF directly caused that the pressure had more remarkable decrease than that of PWCF [22]. Cavitation evolution was facilitated by silt particles (Fig. 6).

5.2 Variations of Turbulent Kinetic Energy

Qualitative comparisons on the distributions of turbulent kinetic energy of PWCF and SPWCF in the nozzle were performed; case of $d_s = 0.0015$ mm and $\alpha_s = 1\%$ was employed. On the other hand, maximum and minimum turbulent kinetic energies were compared quantitatively.

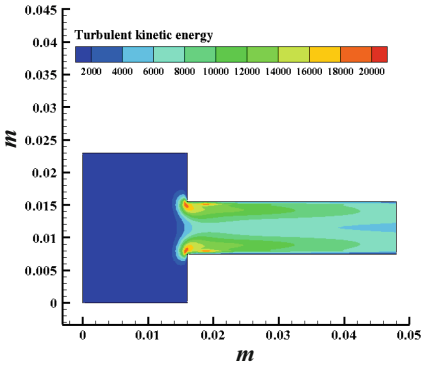

(a) PWCF

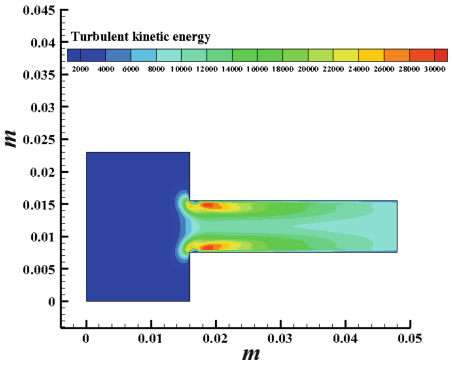

(b) SPWCF (d_s=0.0015mm and α_s=1%)

Fig. 7. Distributions of turbulent kinetic energy.

The identical characteristics were that turbulent kinetic energy with high intensities mainly distributed at the beginning segment of the orifice; it was in accordance with the distributions of high vapor volume fractions. For low intensity condition, they were at the beginning parts of the nozzle (Fig. 7).

Variations of maximum and minimum turbulent kinetic energies of SPWCF under all silt mean diameter conditions are shown in Fig. 8. Numerical simulation results indicated that they were respectively greater than in PWCF. Therefore, pressure in SPWCF had more significantly decrease; silt particles with diverse mean diameters promoted cavitation development in the nozzle.

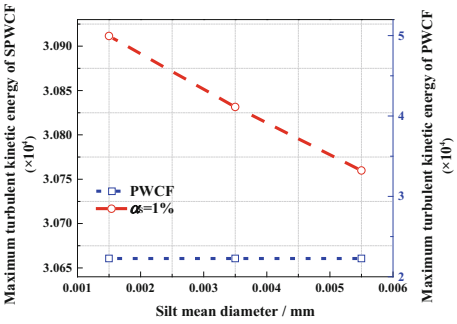

(a) Maximum

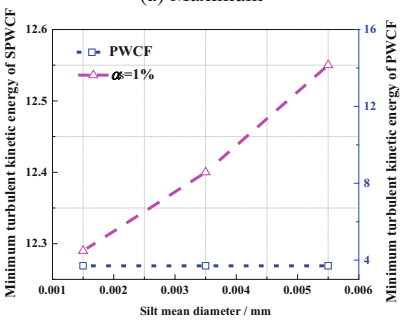

(b) Minimum

Fig. 8. Variations of maximum and minimum turbulent kinetic energies under different silt mean diameter conditions.

6 Conclusions

Effects of different silt particle mean diameters on cavitation evolution in the nozzle were numerically investigated. Vapor contents of PWCF and SPWCF were compared to build the laws to determine the role of silt particle mean diameter. Variations of slip velocity and turbulent kinetic energy were discussed to reveal the mechanisms. Main conclusions were as following:

(1) Vapor content in SPWCF was greater than in PWCF. Silt particles promoted cavitation evolution in the nozzle.
(2) Maximum and minimum slip velocities were higher than the corresponding ones in PWCF.
(3) Maximal and minimal turbulent kinetic energies were greater than those of PWCF.
(4) Slip velocity and turbulent kinetic energy were two primary factors to influence SPWCF development.

Authors' Contributions. Xiangdong Han performed the numerical simulations and wrote the paper. Fangyan Yu analysed the results.

References

1. Koukouvinis, F., Gavaises, M.: Cavitation and Bubble Dynamics: Fundamentals and Applications. Academic Press (2021)
2. Washio, S.: Recent Developments in Cavitation Mechanisms. Elsevier Science & Technology, Woodhead Publishing (2015)
3. Grist, E.: Cavitation and the Centrifugal Pump: A Guide for Pump Users. CRC Press (1998)
4. Kumar, P., Saini, R.P.: Study of cavitation in hydro turbines - a review. Renew. Sustain. Energy Rev. **14**, 374–383 (2010). https://doi.org/10.1016/j.rser.2009.07.024
5. Lešnik, L., Kegl, B., Bombek, G., Hočevar, M., Biluš, I.: The influence of in-nozzle cavitation on flow characteristics and spray break-up. Fuel **222**, 550–560 (2018). https://doi.org/10.1016/j.fuel.2018.02.144
6. Stark, C., Shi, W.C., Troll, M.: Cavitation funnel effect: bio-inspired leading-edge tubercle application on ducted marine propeller blades. Appl. Ocean Res. **116**, 102864 (2021). https://doi.org/10.1016/j.apor.2021.102864
7. Hammitt, F.G.: Cavitation and Multiphase Flow Phenomena. McGraw-Hill Book Company (1980)
8. Han, X.D., Kang, Y., Li, D., Zhao, W.G.: Effects of surface roughness on self-excited cavitating water jet intensity in the organ-pipe: Numerical simulations and experimental results. Mod. Phys. Lett. B **33**(27), 1950324 (2019). https://doi.org/10.1142/S021798491950324X
9. Ronald, Y.F.: Cavitation. Imperial College Press (1999)
10. Wang, L.L., Lu, C.H.: The effect of viscosity on the cavitation characteristics of high speed sleeve bearing. J. Hydrodyn. **27**(3), 367–372 (2015). https://doi.org/10.1016/S1001-6058(15)60494-2
11. Han, X.D., Kang, Y., Zhao, W.G., Sheng, J.P., Li, D.: Silt particles affect cavitation flow: Analyzing variations in silt mean diameter and concentration. Powder Technol. **356**, 671–690 (2019). https://doi.org/10.1016/j.powtec.2019.09.005
12. Zhao, W.G., Han, X.D., Li, R.N., Zheng, Y.J., Wan, Y.Y.: Effects of size and concentration of silt particles on flow and performance of a centrifugal pump under cavitating conditions. Mod. Phys. Lett. B **31**(34), 1750312 (2017). https://doi.org/10.1142/S0217984917503122
13. Zhao, W.G., Han, X.D., Li, R.N., Zheng, Y.J., Pan, X.W.: Effects of silt diameter and silt concentration on cavitation flow in centrifugal pump. Trans. Chinese Soc. Agric. Eng. **33**(4), 117–124 (2017). https://doi.org/10.11975/j.issn.1002-6819.2017.04.017
14. Hu, H.X., Zheng, Y.G.: The effect of sand particle concentrations on the vibratory cavitation erosion. Wear **384–385**, 95–105 (2017). https://doi.org/10.1016/j.wear.2017.05.003
15. Li, S.C.: Cavitation enhancement of silt erosion - an envisaged micro mode. Wear **260**(9–10), 1145–1150 (2006). https://doi.org/10.1016/j.wear.2005.07.002
16. Wu, S.J., Zuo, Z.G., Stone, H.A., Liu, S.H.: Motion of a free-settling spherical particle driven by a laser-induced bubble. Phys. Rev. Lett. **119**, 084501 (2017). https://doi.org/10.1103/PhysRevLett.119.084501
17. Xu, M., Ji, C., Zou, J., Ruan, X., Fu, X.: Particle removal by a single cavitation bubble. Sci. China Phys. Mech. Astron. **57**(4), 668–673 (2014). https://doi.org/10.1007/s11433-013-5192-4
18. Tu, J.Y., Yeoh, G.H., Liu, C.Q.: Computational Fluid Dynamics: A Practical Approach. Elsevier (2007)
19. Wilcox, D.C.: Simulation of transition with a two-equation turbulence model. AIAA J. **32**(2), 247–255 (1994). https://doi.org/10.2514/3.59994
20. Schnerr, G.H., Sauer, J.: Physical and numerical modeling of unsteady cavitation dynamics. In: Proceedings of the 4th International Conference on Multiphase Flow (2001)

21. Nurick, W.H.: Orifice cavitation and its effect on spray mixing. J. Fluids Eng. Trans. ASME **98**(4), 681–687 (1976). https://doi.org/10.1115/1.3448452
22. Zhao, W.G., Han, X.D., Sheng, J.P., Pan, X.W.: Research on the effects of silt mean diameters and silt concentrations on the cavitation flow in a nozzle. J. Shanghai Jiaotong Univ. (China Ed.) **51**(11), 1399–1404 (2017). https://doi.org/10.16183/j.cnki.jsjtu.2017.11.017